Transactions on Engineering Sciences vol 12, © 1996 WIT Press, www.witpress.com, ISSN 1743-3533

Heat transfer and thermal stress calculation in fire-exposed concrete walls

J. Šelih,[a] A.C.M. Sousa[b]

[a]*Civil Engineering Institute ZRMK, Dimičeva 12, 61109 Ljubljana, Slovenia*

[b]*Department of Mechanical Engineering, University of New Brunswick, P.O.Box 4400, Fredericton E3B 5A3, Canada*

Abstract

An analysis which combines heat and mass transport with the calculation of thermal stresses due to non-uniform temperature distribution is presented for a concrete wall exposed to different fire scenarios. The mathematical formulation of simultaneous heat an mass transfer is based on the averaging procedure over a representative elementary volume of the porous medium, and in the thermal stresses calculation, linear elastic strains are assumed.

The results indicate that thermal stresses higher than those resulting from vapour trapped within the material may develop in concrete walls exposed to fire elevated temperatures.

1 Introduction

Exposure to fire is one of the most destructive processes that a concrete structure can be subjected to during its service life. To prevent excessive damage, which may cause the eventual collapse of the structure and even the loss of human lives, safety codes, particularly for buildings, have enforced measures designed to guarantee their integrity and survivability. Usually, they require an assessment of the building material by standard experimental tests [1], however, there is a considerable uncertainty related to fire endurance tests and the fundamental phenomena involved in a fire [2].

Combustion in a closed compartment, as it occurs during a fire in a building, involves highly complex mechanisms. As a first approximation, its influence upon heat transfer to the adjacent structure can be expressed by a

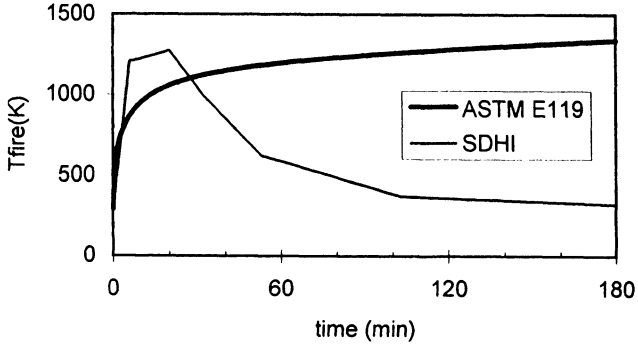

Figure 1 Fire exposure curves according to a) ASTM E-119 standard [1], and b) Ellingwood [2] (SDHI=short duration high intensity fire exposure curve).

time dependent fire temperature. Several time dependent relations to describe it have been proposed in the literature, e.g. [1], [2]. The curve imposed by [1] is a conservative estimate of an actual fire, since fire temperature keeps increasing with time, which implies an inexhaustible supply of fuel during the fire. On the other hand, in [2], a curve is proposed which is obtained by using an overall energy balance equation for the fire compartment. This curve exhibits an early peak of temperature followed by a decaying period, where the fire temperature decreases. Both types of fire exposure curves are presented in Figure 1.

Concrete is a porous material, with its pores filled with water. Elevated temperatures occurring in a concrete structure during fire affect moisture migration within the porous material. Heat supplied from the fire is being partly absorbed by the evaporation of the liquid water. If the evaporation rate is higher than the rate of the vapour migration, high pore pressures may develop. If they exceed the tensile strength of the material composing the solid matrix, explosive spalling and eventual collapse of the structure may occur. Experimental evidence corroborating the occurrence of these catastrophic events for normal weight and lightweight concrete with high moisture content was reported in [3]. Spalling seems to be closely related to water phase changes and moisture migration in the material, and high moisture contents may therefore result in a higher risk of explosive spalling during a fire. In addition to explosive spalling, the stresses which develop as a result of the non-uniform temperature distribution may cause serious material failure [4].

Concrete walls belong to the most frequently employed structural elements in buildings, and due to their large contact area with fire, their behaviour contributes significantly to the overall thermal and structural response of a building in fire.

The objective of the present study is to enhance the capability of the existing numerical tool for fire safety assessment of concrete structures [5] by implementing the calculation of the thermal stresses within a concrete wall, as proposed in [4].

The wide distribution of pore size encountered in concrete yields large specific internal areas as high as 10 m^2/g [6] resulting in a considerable proportion of adsorbed liquid water. A physically realistic mathematical formulation for mass and heat transfer in concrete has to describe free water flow, adsorbed (bound) water movement, water vapour and air migration, and the effects of water phase change. Whitaker's formulation [7] was extended to include adsorbed water movement by Perre and Degiovanni [8], and since this work meets most of the requirements specified above, it was used as the base for the numerical model for heat and mass transfer employed.

2 Mathematical formulation

2.1 Governing equations of heat and mass transfer in porous medium

The details of the mathematical formulation developed to describe heat and mass transfer in concrete are fully described in [9], and only the main features are given here. The volumetric fractions for the liquid (l), bound (b), gaseous (g) and solid (s) phase are linked by the following volumetric constraint:

$$\varepsilon_l + \varepsilon_g + \varepsilon_b + \varepsilon_s = 1 \tag{1}$$

The solid phase, as a sensible approximation, is assumed constant in the mass transfer calculation.

Conservation of mass for the liquid and bound water, and water vapour requires

$$\frac{\partial}{\partial t}(\rho_l(\varepsilon_l + \varepsilon_b) + \varepsilon_g \overline{\rho}_1^g) + \nabla(\rho_b \overline{\mathbf{v}}_\mathbf{b} + \rho_l \overline{\mathbf{v}}_\mathbf{l} + \overline{\rho}_1^g \overline{\mathbf{v}}_\mathbf{l}) = 0 \tag{2}$$

where $\overline{\mathbf{v}}_\mathbf{l}$ indicates the averaged velocity vector, and ρ_l the density of the liquid phase. $\overline{\rho}_1^g \overline{\mathbf{v}}_\mathbf{l}$ is the mass flux of the water vapour, and $\rho_b \overline{\mathbf{v}}_\mathbf{b}$ the mass flux of the bound phase. $\overline{\rho}_1^g$ is the intrinsic average of the partial water vapour density over the gaseous phase.

The continuity equation for water vapour is written as

$$\frac{\partial}{\partial t}(\overline{\rho}_1^g \varepsilon_g) + \nabla(\overline{\rho}_1^g \overline{\mathbf{v}}_\mathbf{l}) = \overline{m}_l + \overline{m}_b \tag{3}$$

where $\overline{m}_l$ is the evaporation rate of the liquid, and $\overline{m}_b$ the evaporation rate of the bound phase. Darcy's law is used to describe the velocities of both liquid and gas phase, and with low relative values of the water vapour partial pressure as compared to those for the total gaseous pressure, the assumption that the mixture behaves as an ideal gas is adopted.

The thermal energy equation that includes the term describing the phase change and convective heat transfer is formulated as

$$(\rho c_p)\frac{\partial \overline{T}}{\partial t} + ((c_p)_l \rho_l \overline{\mathbf{v}}_l + (c_p)_l \overline{\rho}_b \overline{\mathbf{v}}_b + \rho_g^g c_p^g \overline{\mathbf{v}}_g)\cdot \nabla \overline{T} + \Delta h_{vap}(\overline{m}_l + \overline{m}_b) + h_s \overline{m}_b - \overline{\rho}_b \overline{\mathbf{v}}_b \cdot \nabla h_s = \nabla(\lambda_{eff} \nabla \overline{T}) \quad (4)$$

where Δh_{vap} is the specific heat of evaporation, h_S the differential heat of sorption, λ_{eff} the effective thermal conductivity, and ρc_p represents the averaged product of the density by the specific heat.

The exchange coefficients of heat and mass transfer, α and β, are taken as constant, and the total heat flux on the fire-exposed surface can be written as

$$((\lambda_{eff} \nabla \overline{T}) + \Delta h_{vap}(\rho_l \overline{\mathbf{v}}_l + \overline{\rho}_b \overline{\mathbf{v}}_b) - \overline{\rho}_b \overline{\mathbf{v}}_b \cdot h_s)\cdot \mathbf{n}_{boun} = \alpha(\overline{T} - T_\infty) + \sigma e(\overline{T}^4 - T_\infty^4) \quad (5)$$

where $\mathbf{n}_{boun}$ is the unit vector normal to the boundary surface, and T_∞ the ambient temperature. σ is the Stefan-Boltzmann constant, and e is the emissivity. A similar convective type of boundary condition is used for the mass flux, namely:

$$(\rho_l \overline{\mathbf{v}}_l + \overline{\rho}_b \overline{\mathbf{v}}_b + \overline{\rho}_l^g \overline{\mathbf{v}}_l)\cdot \mathbf{n}_{boun} = \beta(\overline{\rho}_l^g - \rho_{l\infty}) \quad (6)$$

$\rho_{l\infty}$ the partial water vapour density of the ambient, which remains constant throughout the fire exposure.

The total gaseous pressure at the fire-exposed surface is taken as equal to the atmospheric pressure. In the beginning of the process, temperature, gas phase pressure and saturation are assumed to be uniform throughout the wall.

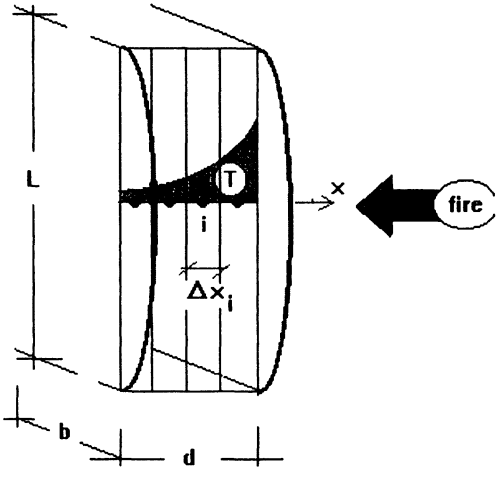

Figure 2 Schematic depiction of the concrete wall exposed to fire.

2.2 Discretization of governing equations

The control volume formulation [10] is employed in order to discretize in space the governing differential equations, and a fully implicit scheme is employed for the integration in time. The coefficients appearing in the governing equations are strongly dependent upon the variables to be computed, therefore, an iterative procedure is required within each time step. The set of linearized equations is solved in each sweep of the iterative procedure by using the alternating direction block iterative method, and the tridiagonal matrix algorithm (TDMA) [10] is used as a segregated solver for each equation. Results of the code are generated in terms of spatial distribution of temperature, saturation and total pressures of the gas phase at a pre-specified time.

2.3 Calculation of stresses resulting from non-uniform temperature distribution

To calculate the thermal stresses in the concrete wall, the cross-section is divided into n layers as shown in Figure 2. It is assumed that the vertical movement of each layer is prevented. The stress in layer i, which has a thickness Δx_i , is determined by

$$\sigma_{1,i} = -\alpha_{T,i} E_i (T_i - T_i^0) \tag{7}$$

where $\alpha_{T,i}$ is the thermal expansion coefficient, E_i modulus of elasticity, and T_i and T_i^0 current and initial temperature of layer i, respectively.

Vertical movement is prevented, therefore the force acting on the entire cross-section is

$$F = -\Sigma \sigma_i A_i' = \sigma_2 A' \tag{8}$$

where A_i' is the reduced area of the layer i, $A_i' = b \Delta x_i \xi_i$, and A' the total area of the cross-section, $A' = \Sigma A_i'$. Externally applied stress $\sigma_2 = F/A'$ is acting on each layer. ξ_i is the reduction factor that accounts for the changes of modulus of elasticity due to the increase of temperature:

$$\xi_i = E(T_i) / E_{ref} \tag{9}$$

E_{ref} is the reference modulus of elasticity at 20°C.

Moment of inertia of the entire reduced cross-section is

$$I = \sum_i (A_i' y_i^2 + \Delta x_i^{\,2} \xi_i b/12) \tag{10}$$

where y_i is the distance from the layer i to the centre of gravity.

$$y_i = |x_{CG} - x_i| \tag{11}$$

The distance to the centre of gravity is determined with the expression

$$x_{CG} = (\Sigma A_i' x_i) / A' \tag{12}$$

where x_i is the distance to the layer i.

The additional bending moment, M, defined with

$$M = \sum_i (\sigma_{1,i} + \sigma_2)\, y_i A_i' \tag{13}$$

yields a stress condition

$$\sigma_{3,i} = \frac{M y_i}{I} \tag{14}$$

The total stress due to the non-uniform temperature distribution in the layer i is defined as

$$\sigma_i = \sigma_{1,i} + \sigma_2 + \sigma_{3,i} \tag{15}$$

3 Results and discussion

The analysis of a 0.2 m thick lightweight concrete wall, as depicted in Figure 2 was performed for both types of fire-exposure curves presented in Figure 1. Heat and mass fluxes on both sides of the wall are defined by Eqs. (5) and (6). The initial ambient temperature and relative humidity are taken as 20°C and 30%, respectively, on both sides of the wall. Ambient conditions adjacent to the wall not exposed to fire are assumed constant, and at the fire-exposed side, the ambient temperature increases according to the selected exposure curve. The mass transfer coefficient is taken as 0.01 m/s, and the heat transfer coefficient and emissivity have the value of 20 W/(mK) and 0.5 on both sides of the wall, respectively. The initial saturation and temperature in the wall are 90% and 20°C, respectively.

The capillary pressure dependence upon saturation follows the Leverett approach [11]. The relative permeabilities of the gas and liquid phase are also taken as proposed in [11], with a modification in the high saturation domain, suitable for concrete, where the gas permeability has a small nonzero value in the high saturations domain. The specific permeability of concrete is taken as 5 10^{-16} m^2 [12]. The functions for the sorption isotherm and bound water diffusion coefficient are selected in such a way that they depend on one single parameter, the irreducible saturation. The details on the selection of the constitutive relations, mass transfer coefficient, permeability, porosity and irreducible saturation levels are given in [9].

The dependence of the modulus of elasticity upon temperature, $E(T)$, is depicted in Figure 3, and the thermal expansion coefficient α_T is taken as constant with the value of 1.3 10^{-5} K^{-1} [13].

Figure 4 presents the saturation, temperature and gas pressure distribution in the wall exposed to fire for both fire scenarios for exposure times of 22 and 45 minutes. For the SDHI fire [2], the temperature reaches its peak at the exposed surface after 22 minutes of exposure. Temperature at this surface reaches approximately the same value after 45 minutes of exposure

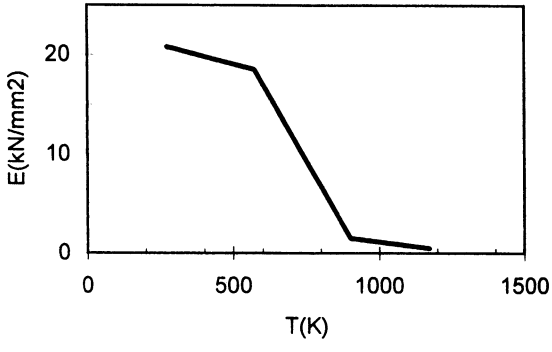

Figure 3 Dependence of the modulus of elasticity upon temperature for concrete [13].

according to ASTM E-119 [1]. The temperature distribution within the wall, however, is different for the two cases, and the temperature 0.05 m away from the exposed surface is approximately 70 K higher after 45 minutes of ASTM E-119 exposure compared to the wall exposed to SDHI fire for 22 minutes. The fire rate in the initial stage is higher for the SDHI exposure as compared to the ASTM E-119 exposure, the drying of the wall proceeds faster and at 22 minutes, the hygroscopic region is larger for the case of SDHI fire exposure. Gas pressures reach their maximum values at the transition value between liquid flow and hygroscopic region, the irreducible saturation. As expected, the maximum values for gas pressures increase with time when the wall is exposed to ASTM E-119 fire exposure. The same phenomenon is observed for the wall subjected to the SDHI type of fire.

Stresses induced by the non-uniform temperature distribution in the wall are depicted in Figure 5. At peak temperatures, occurring at 45 minutes for ASTM E-119, and 22 minutes for SDHI fire exposure, a thin layer of the wall next to the exposed surface is in tension due to the reduced modulus of elasticity. Tensile stresses in that region are very high due the large increase of the temperature combined with the assumption of linear elastic strains in the thermal stresses calculation. When temperatures are below the maximum values (at 22 minutes for ASTM, and 45 minutes for SDHI fire exposure), layers next to both surfaces are in compression. For all cases analysed, the central part of the wall is in tension.

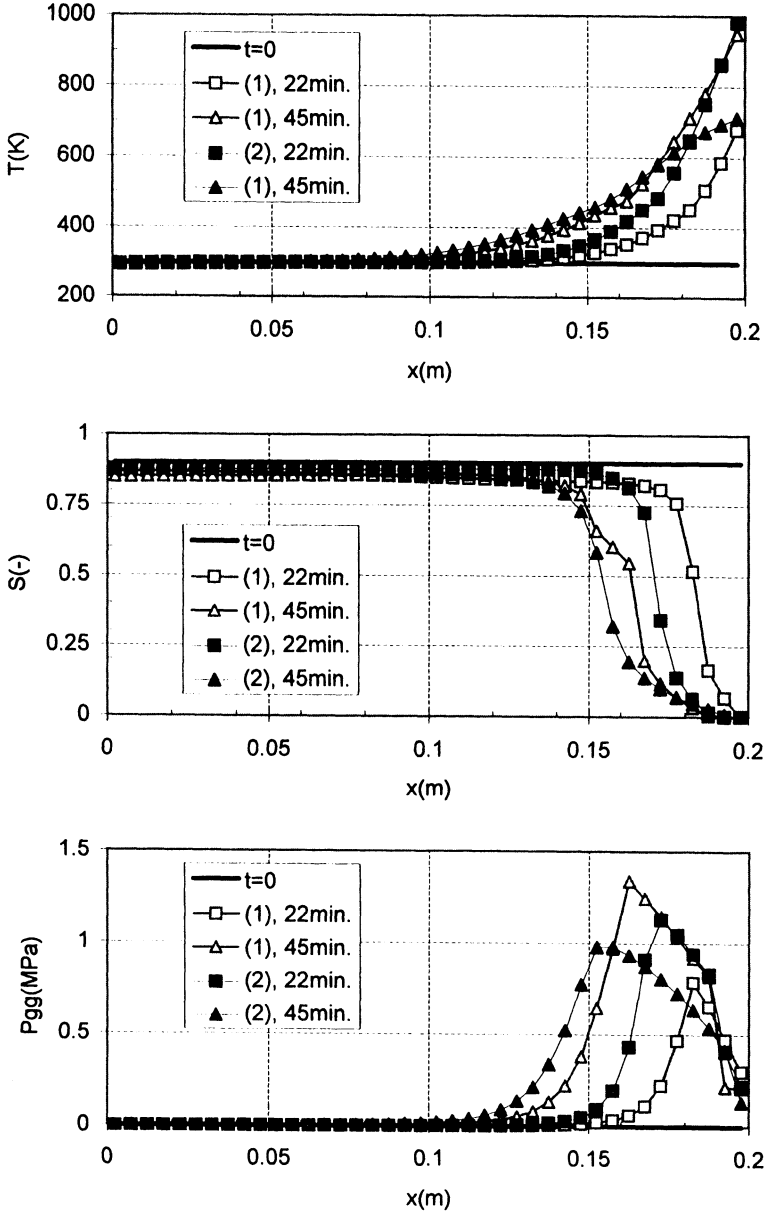

Figure 4. a) Temperature (T), b) saturation (S), and c) gas pressure ($\overline{p}_g^g$) distribution in a wall exposed to fire exposure according to ASTM E-119 standard [1], and Ellingwood [2] at 22 and 45 minutes.

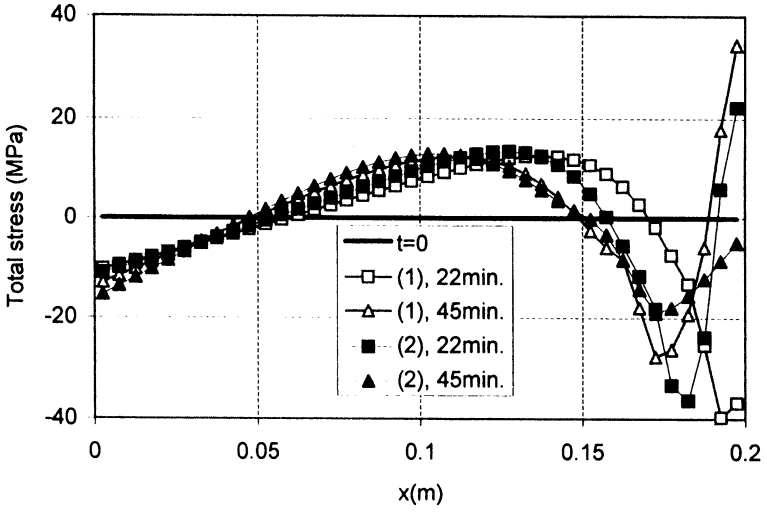

Figure 5 Total thermal stress distribution in a wall exposed to fire exposure according to ASTM E-119 standard [1], and Ellingwood [2] at 22 and 45 minutes.

4 Concluding remarks

The numerical model presented has the capability of providing a simultaneous, time-dependent analysis of heat and mass transfer combined with the computation of thermal stresses due to a non-uniform temperature distribution. The submodel for the calculation of the thermal stresses makes the assumption of linear elastic deformations due to the temperature differentials. Results are presented for a concrete wall subjected to two extreme cases of fire scenario, i.e. fire exposure according to the ASTM E-119 standard, and to short duration high intensity (SDHI) type of fire.

The results show that the type of fire scenario has a major influence upon the saturation and temperature development within the wall, and consequently upon the thermal stresses. These stresses, under the simplifying and somewhat conservative assumptions made are much higher than the internal pressures developed in the pores. On a preliminary basis, and under the assumptions made and chosen fire scenarios, it can be advanced that thermal stresses rather than internal pressures will pose the single largest risk to the integrity of the structure.

5 Acknowledgement

Partial funding received from a Natural Sciences and Engineering Research Council of Canada operating grant OGP0001398 awarded to A.C.M. Sousa is acknowledged.

6 References

1. "*Standard test methods for fire test of building construction and materials*", ASTM Standard E-119, ASTM, Philadelphia, Pa., 1989.
2. Ellingwood B.R., Impact of fire exposure on heat transmission in concrete slabs, *J. Struct. Engrg., ASCE*, Vol.117(6), pp.1870-1875, 1991.
3. Copier, W.J., The spalling of the normal weight and lightweight concrete exposed to fire, *Fire safety of concrete structures*, ACI Publication SP-80, American Concrete Institute, Detroit, Mich., pp.219-237, 1983.
4. Lenczner, D., *Movements in buildings*, Pergamon Press, New York, 1981.
5. Šelih, J., Sousa, A.C.M., & Bremner T.W., Moisture and heat flow in concrete walls exposed to fire, *J. Engrg. Mech., ASCE*, Vol.120(19), pp. 2028-2043, 1994.
6. Daian, J.F., Condensation and isothermal water transfer in cement mortar: Part I - pore size distribution, equilibrium water condensation and imbibition, *Transport in Porous Media*, Vol.3, pp.563-589, 1988.
7. Whitaker, S., Simultaneous heat, mass, and momentum transfer in porous media: a theory of drying, *Adv. in Heat Transfer*, Vol.13, pp.119-200, 1977.
8. Perre, P., & Degiovanni, A., Simulation par volumes finis des transférts couplés en milieux poreux anisotropès: séchage du bois à basse et à haute temperature, *Int. J. of Heat & Mass Tr.*, Vol.33, pp.2463-2478, 1990.
9. Šelih, J., *Movement of water during drying of saturated concrete*, Ph.D. Thesis, University of New Brunswick, Fredericton, Canada, 1994.
10. Patankar, S.V., *Numerical heat transfer and fluid flow*, Hemisphere Publ. Corp., New York, NY, 1980.
11. Scheidegger, A.E., *The physics of flow through porous media*, University of Toronto Press, Toronto, Canada, 1974.
12. Mehta, P.K., *Concrete: structure, properties and materials*, Prentice Hall Inc., Englewood Cliffs, NJ, 1986.
13. Keats, C., M.Sc. Thesis, *Effect of elevated concrete on concrete*, University of New Brunswick, Fredericton, Canada, 1994.